Atmos. Meas. Tech. Discuss., 8, 9959–9992, 2015
www.atmos-meas-tech-discuss.net/8/9959/2015/
doi:10.5194/amtd-8-9959-2015

Atmospheric Measurement Techniques Discussions
Open Access

A microwave satellite water vapour column retrieval for polar winter conditions

C. Perro[1], G. Lesins[1], T. Duck[1], and M. Cadeddu[2]

[1]Dalhousie University, Halifax, Nova Scotia, Canada
[2]Argonne National Laboratory, Argonne, IL, USA

Received: 10 June 2015 – Accepted: 26 August 2015 – Published: 24 September 2015

Correspondence to: C. Perro (christopher.perro@dal.ca)

Published by Copernicus Publications on behalf of the European Geosciences Union.

Abstract

A new microwave satellite water vapour retrieval for use in polar winter conditions is presented. The retrieval employs a priori information and an iterative approach. It is tested using simulated and actual measurements from the Microwave Humidity Sounder (MHS) satellite instruments. Ground truth is provided by the G-band vapor radiometer (GVR) at Barrow, Alaska. For water vapour columns less than 6 $kg\,m^{-2}$, comparison with the GVR gives a standard deviation of 0.39 $kg\,m^{-2}$ and a systematic bias of 0.08 $kg\,m^{-2}$. The errors are shown to be significantly less than for other satellite measurement systems. The errors are comparable to those from atmospheric reanalyses; however, the MHS data come at much higher horizontal resolution (< 40 km) and are shown to reveal more structure. The retrieval can be used to obtain pan-Arctic maps of water vapour columns of unprecedented quality. The retrieval may also be applied to the Special Sensor Microwave Imager/Sounder (SSMIS) and the Advanced Technology Microwave Sounder (ATMS).

1 Introduction

The polar winter troposphere is very dry, having water vapour columns typically around 3 $kg\,m^{-2}$ (Serreze et al., 1995). Climate change, which is amplified at high latitudes, is expected to increase absolute humidity and alter the radiative balance (Stamnes et al., 1998) with consequences for global climate and Arctic sea ice. Although there are few ground-based measurements of water vapour in the polar regions, microwave instruments aboard a series of polar-orbiting satellites since 1991 (F11 to 19, NOAA-15 to 19, MetOP-A and B, FY3-A to C, and NPP) provide a substantial data set. Planned missions with microwave instruments include JPSS-1 and 2, MetOP-C, and DMSP-S20. Microwave measurements are advantageous over infrared or visible because clouds do not absorb and scatter microwave radiation to the same degree. This allows for measurements of water vapour in most weather conditions (Miao et al., 2001).

AMTD
8, 9959–9992, 2015

This paper introduces a modified technique for retrieving water vapour columns from microwave satellite measurements in polar winter conditions which are characterized by low optical depths. The retrieval uses the microwave signal formulation given by Miao (1998) (hereafter referred to as M98). M98's retrieval technique involves several approximations that were somewhat relaxed in a variation by Melsheimer and Heygster (2008) (hereafter referred to as MH08). Our retrieval (hereafter referred to as PLDC15) employs fewer approximations than either M98 or MH08, but requires a priori data for atmospheric conditions. The results are more accurate, but come at the cost of an increase in computational complexity.

The MH08 and PLDC15 retrievals are tested against simulated signals in order to determine sources of error. Their performance is also assessed using Microwave Humidity Sounder (MHS) measurements from MetOP-A and NOAA-18 in comparison with surface based G-band vapor radiometer (GVR) measurements at Barrow, Alaska (71.3° N, 156.8° W). MHS measurements were chosen because they provide the longest period of overlap with the GVR, with continuous water vapour column measurements since 2005 (Cadeddu et al., 2009). The GVR measures brightness temperatures at four double-sideband frequencies near the 183 GHz water vapour absorption line. The water vapour column is estimated to have less than 5 % error for values between 1 and 8 $\mathrm{kg\,m^{-2}}$ (Cadeddu et al., 2009). Comparisons of water vapour columns less than 8 $\mathrm{kg\,m^{-2}}$ for the GVR and Vaisala radiosondes launched from the ARM Climate Research Facility in Barrow, Alaska have a standard deviation of 0.23 $\mathrm{kg\,m^{-2}}$.

Similar to the GVR, the MHS instruments measure microwave radiances at five frequencies near the 183 GHz water vapour absorption line. MHS is the successor to AMSU-B, the target instrument for MH08's analysis. The specifications for both instruments are summarized in Table 1. The main difference between the two is the decreased noise for each channel of the MHS.

The structure of this paper is as follows. Section 2 introduces M98's microwave signal formulation and three techniques (M98, MH08, and PLDC15) for retrieving water vapour column values. Section 3 describes how different frequency regimes are

AMTD
8, 9959–9992, 2015

treated. Comparisons between the PLDC15 and MH08 retrievals using simulated signals are given in Sect. 4. Section 5 follows by comparing the PLDC15 retrieval with the GVR, other satellite instruments (AIRS and MIRS) and atmospheric reanalysis data sets (ECMWF Interim, NCEP, ASR, and JRA-55). The results are discussed in Sect. 5.3.

2 Microwave signal formulation and retrieval techniques

The brightness temperature T_i measured at frequency ν_i by channel i of a satellite-borne microwave instrument is given by

$$T_i = m_p(\nu_i)T_s - (T_o - T_c)(1-\varepsilon_i)\,e^{-2\tau_i \sec\theta} \tag{1}$$

where T_s is the skin temperature, T_o is the atmospheric surface temperature, T_c is the cosmic background temperature, ε_i is the surface emissivity, $\tau_i \equiv \tau_i(0,\infty)$ is the total optical depth, θ is the zenith viewing angle of the satellite, and m_p is a factor incorporating the vertical structure of the atmosphere. Equation (1) is a combined form of the upwelling and downwelling brightness temperature equations that includes a contribution from cosmic microwave background radiation. The solar contribution to the microwave background is ignored and microwave contributions are assumed to be identical in both polarizations. The surface is also assumed to be a perfect specular reflector (Guissard and Sobieski, 1994).

Following M98, but without making approximations, equations for brightness temperatures T_1, T_2, T_3 in three channels can be combined to obtain

$$\frac{\Delta T_{12} - b_{12}}{\Delta T_{23} - b_{23}} = \frac{r_1}{r_2}\left(\frac{e^{-2\tau_1\sec\theta} - (r_2/r_1)e^{-2\tau_2\sec\theta}}{e^{-2\tau_2\sec\theta} - (r_3/r_2)e^{-2\tau_3\sec\theta}}\right) \tag{2}$$

where $\Delta T_{12} = T_1 - T_2$ and $\Delta T_{23} = T_2 - T_3$ are brightness temperature differences, and r_1, r_2, and r_3 are surface reflectances with $r = 1 - \varepsilon$. The factors b_{12} and b_{23}, are bias

AMTD
8, 9959–9992, 2015

coefficients (Miao, 1998; Melsheimer and Heygster, 2008) given by

$$b_{ij} = \int_0^\infty \left(e^{-\tau_j(z,\infty)\sec\theta} - e^{-\tau_i(z,\infty)\sec\theta}\right)\frac{\mathrm{d}T(z)}{\mathrm{d}z}\mathrm{d}z$$
$$+ (T_\mathrm{o} - T_\mathrm{s})\left(\varepsilon_j e^{-\tau_j\sec\theta} - \varepsilon_i e^{-\tau_i\sec\theta}\right)$$
$$+ r_j e^{-2\tau_j\sec\theta}\int_0^\infty \left(1 - e^{\tau_j(z,\infty)\sec\theta}\right)\frac{\mathrm{d}T(z)}{\mathrm{d}z}\mathrm{d}z$$
$$- r_i e^{-2\tau_i\sec\theta}\int_0^\infty \left(1 - e^{\tau_i(z,\infty)\sec\theta}\right)\frac{\mathrm{d}T(z)}{\mathrm{d}z}\mathrm{d}z \quad (3)$$

where $\tau(z,\infty)$ is the optical depth above altitude z.

The three retrieval techniques (M98, MH08, and PLDC15) used to solve for the water vapour column are described next. The retrieval techniques are subject to frequency regime and reflectance choices, and these are discussed in Sect. 3.

2.1 M98

The M98 retrieval simplifies the formulation of Eqs. (2) and (3). It is assumed that the frequencies for each measurement are similar enough that $r_1 = r_2 = r_3$, and all but the first term in Eq. (3) is neglected. It is also assumed that the optical depth depends linearly on the water vapour column. This allows a series expansion of Eq. (2) to yield

$$W\sec\theta = C_0 + C_1\log\left(\frac{\Delta T_{12} - b_{12}}{\Delta T_{23} - b_{23}}\right) \quad (4)$$

where W is the water vapour column, and C_0 and C_1 are coefficients that combine integrated mass absorption coefficients. Notice that the dependence on surface emissivity is eliminated.

AMTD
8, 9959–9992, 2015

M98 assumed constant coefficients b_{12}, b_{23}, C_0 and C_1, and determined them using a 1-D radiative transfer model with radiosonde profile inputs. A separate calibration is required for each frequency triplet ν_1, ν_2, ν_3.

2.2 MH08

MH08 proposed a variation of the M98 retrieval for cases with water vapour columns greater than $8\,\mathrm{kg\,m^{-2}}$. Instead of assuming all reflectances to be the same, they allow for the possibility that r_1 differs from $r_2 = r_3$. Following M98, a series expansion of Eq. (2) gives

$$W \sec\theta = C_0 + C_1 \log\left[\frac{r_2}{r_1}\left(\frac{\Delta T_{12} - b_{12}}{\Delta T_{23} - b_{23}} + C\right) - C\right]. \quad (5)$$

MH08 found C to be constant for the range of water vapour columns under consideration. The coefficients b_{12}, b_{23}, C_0, and C_1 were determined using the same approach as in M98 except with a viewing angle dependence. A separate calibration is required for each frequency triple ν_1, ν_2, ν_3. Aircraft measurements of sea ice emissivity were used to establish a constant value for r_2/r_1.

2.3 PLDC15

Our approach is to employ Eqs. (2) and (3), but with fewer assumptions. Like M98 and MH08 we assume that water vapour is the only significant absorber in the frequency range of interest, and neglect the influence of liquid clouds and ice crystals. Although liquid water is a strong absorber, the absorption is divided out in the retrieval (Miao et al., 2001), and so a water vapour column may still be obtained in optically-thin conditions. Values for the reflectances r_1, r_2 and r_3 are assumed, and this is discussed further in Sect. 3.

As a practical matter, the second term in Eq. (3) is ignored. The second term in Eq. (3) is proportional to the difference between the skin and surface air temperatures,

AMTD
8, 9959–9992, 2015

and comparisons between atmospheric reanalysis products for this factor show considerable disagreement. We also take $r = r_i = r_j$ in the third and fourth terms of Eq. (3), leaving

$$b_{ij} \approx \int_0^\infty \left(e^{-\tau_j(z,\infty)\sec\theta} - e^{-\tau_i(z,\infty)\sec\theta}\right)\frac{\mathrm{d}T(z)}{\mathrm{d}z}\mathrm{d}z$$
$$+ r\left[e^{-2\tau_j\sec\theta}\int_0^\infty \left(1 - e^{\tau_j(z,\infty)\sec\theta}\right)\frac{\mathrm{d}T(z)}{\mathrm{d}z}\mathrm{d}z\right.$$
$$\left. - e^{-2\tau_i\sec\theta}\int_0^\infty \left(1 - e^{\tau_i(z,\infty)\sec\theta}\right)\frac{\mathrm{d}T(z)}{\mathrm{d}z}\mathrm{d}z\right]. \quad (6)$$

The sensitivity of our retrieval to these assumptions and approximations is evaluated in Sect. 4.4.

Next, we suppose that the optical depth profile $\tau(z,\infty)$ is related to a trial profile $\tau_n(z,\infty)$ by

$$\tau(z,\infty) = x_n\tau_n(z,\infty), \quad (7)$$

where x_n is a scaling factor and $n = \{0,1,2,3,\ldots\}$ is the iteration number. The trial optical depth profile is determined using

$$\tau_n(z,\infty) = \int_z^\infty k\left(p_0(z),T_0(z)\right)w_n(z)\mathrm{d}z \quad (8)$$

where a priori estimates of pressure p_0 and temperature T_0 are required, w_n is the trial water vapour profile, and k is the mass absorption coefficient. For the first iteration ($n = 0$) we take the trial profile w_0 from the a priori estimate. We use the RTTOV

AMTD
8, 9959–9992, 2015

1-D radiative transfer model (Matricardi and Saunders, 1999) to calculate $\tau_n(z,\infty)$. The a priori estimate of the temperature profile is also used to estimate $\mathrm{d}T(z)/\mathrm{d}z$ in Eq. (6).

The scaling factor for each iteration is determined by solving Eqs. (2), (6) and (7) with a numerical nonlinear optimizer. Trial water vapour profiles for iterations $n = \{1,2,3,\ldots\}$ are determined using

$$w_{n+1}(z) = x_n w_n(z). \tag{9}$$

Having obtained the scaling factor, the water vapour column is given by

$$W = x_n \int_0^\infty w_n(z)\mathrm{d}z. \tag{10}$$

Notice that unlike M98 or MH08 there is no need to perform a separate frequency calibration. We stop iterating when the change in the water vapour column is less than 0.1 % between iterations. The number of iterations varies for each measurement and a maximum of 20 iterations is applied. Figure 1 summarizes the PLDC15 retrieval process.

3 Regime selection

To retrieve water vapour columns from microwave data, strongly absorbed frequencies are used to measure small water vapour columns, and weakly absorbed frequencies are used to measure large ones. Three sets of frequencies are used for the MHS, giving rise to the "low", "mid", and "extended" regimes, as summarized in Table 2. M98 uses only the low and mid regimes while MH08 and PLDC15 apply to all three. The retrievals use different criteria for choosing between regimes.

Brightness temperatures typically increase with increasing water vapour column until they maximize and then begin to decrease as the satellite predominantly views an

AMTD
8, 9959–9992, 2015

upper portion of the atmosphere with less sensitivity near the surface. M98 therefore switches from the low to the mid regime when $\Delta T_{12} > 0$ or $\Delta T_{23} > 0$. MH08 switches to a less absorbing regime if $\Delta T_{12} - b_{12} > 0$ or $\Delta T_{23} - b_{23} > 0$.

A difficulty with the above approach is that brightness temperatures are strongly affected by temperature profile structure, and in particular by surface temperature inversions that are ubiquitous during polar winter (e.g., Lesins et al., 2010, 2012). This causes regime selection artifacts, as will be demonstrated in Sect. 4.1.

We take a different approach. The slant water vapour column is determined from a priori information, with the slant given by the instrument's viewing angle. The low regime is used for slant water vapour columns between 0 and 2.5 kg m^{-2}, the mid regime is used from 1.5 to 9 kg m^{-2}, and the extended regime is used above 8 kg m^{-2}. The boundaries of the regimes were chosen by comparing multiple GVR and PLDC15 water vapour columns. When a regime becomes too moist for its strongest absorbing frequency, the retrieval shows a decrease in sensitivity with increasing water vapour. By comparing the standard deviation and bias for adjacent regimes the most optimal regime for a particular range of water vapour column was chosen. Weighted averages are used where regimes overlap in order to smooth the transition. Measurements near the lower boundary of a regime sometimes do not have a solution, and in this case the nearest regime in terms of the slant water vapour column is used.

MH08 retrievals in the low and mid regimes assume $r_1 = r_2 = r_3$, and as such it is equivalent to M98 in those regimes. For the extended regime, the reflectance r_1 is taken to be different from $r_2 = r_3$ because of the separation in frequencies. MH08 found a ratio $r_2/r_1 = 1.22$ from the Surface Emissivities in Polar Regions Polar Experiment (SEPOR/POLEX) aircraft campaign measurements. It is important to note that this value is fixed in their retrieval because it is used in the determination of the constants C_0 and C_1 in Eq. (5).

For the PLDC15 retrieval, we assume $r_1 = r_2 = r_3$ in the low regime, r_1 different from $r_2 = r_3$ in the mid regime, and all three reflectances different in the extended regime. Because there are no pre-determined coefficients in our retrieval, we are able to set

AMTD
8, 9959–9992, 2015

the reflectance ratios according to the appropriate surface type. Different assumptions were made for the simulations and measurement retrievals, as will be explained.

4 Theoretical retrieval performance

To compare the retrieval techniques, we used the RTTOV 1-D radiative transfer model to simulate brightness temperature measurements, employing operational radiosonde profiles from Barrow, Alaska as inputs. A total of 1490 profiles between December and March for 2008 to 2014 were used. The maximum water vapour column was 15 $\mathrm{kg\,m^{-2}}$.

All simulations assumed nadir satellite measurements, and the surface air and skin temperatures were taken to be equal. The surface emissivity was set to 0.8 for all frequencies. Simulations at different viewing angles show insignificant differences in the retrieval of the water vapour column.

RTTOV is used to provide brightness temperatures for both the MHS and AMSU-B instruments. We used AMSU-B simulations for MH08's retrieval given that their retrieval coefficients are calibrated for that instrument. MHS simulations were used for our retrieval.

The retrieval techniques were tested against three different cases, with results given in Sects. 4.1–4.3:

1. simulated signals with no detector noise and a perfect a priori for the atmospheric conditions;
2. simulated signals with detector noise and a perfect a priori for the atmospheric conditions; and
3. simulated signals with detector noise and a climatological a priori for the atmospheric conditions.

In each case we compare the retrieved water vapour columns against the input columns. The simulations are also used to evaluate the impacts of our assumptions

AMTD
8, 9959–9992, 2015

in Sect. 4.4, and to evaluate the possibility of applying the MH08 retrieval to MHS measurements in Sect. 4.5.

4.1 Case 1

The first case tests the intrinsic accuracy of each retrieval by using noiseless simulated signals and perfect a priori knowledge. Figure 2 compares mid regime retrievals (2.5 to 8 kg m^{-2}, excluding overlap) to simulated water vapour columns. Standard deviation and bias values are given in Table 3. The PLDC15 retrieval has negligible standard deviation and bias. This is expected given the ideal conditions for the test, with non-zero values arising from profile interpolation and integration effects in RTTOV. The greater scatter and bias values for MH08 are due to the inherent error in that retrieval's constant coefficients.

In this case, the reduction of standard error by PLDC15 over MH08 is due entirely to the calculation of bias coefficients. Iterations have an insignificant effect on the retrieval.

Figure 3 shows results for the three combined regimes. The MH08 retrieval shows significant bias at the boundary between the low and mid regimes (2.5–3 kg m^{-2}). It can also be seen that the mid regime extends up to approximately 10 kg m^{-2}, which is where the extended regime should be used.

Table 3 summarizes the low, mid, and extended regime results for both retrievals. Similar to the mid regime, the standard deviation for the PLDC15 low and extended regimes is significantly less than for MH08. There is a positive bias in the extended regime of the PLDC15 retrieval and this is due to the assumption that there is no other significant absorber besides water vapour. At 89 GHz, absorption from an oxygen absorption line (118.75 GHz) is not insignificant and causes a small bias.

The results indicate that the error for PLDC15 is lower than for MH08. The PLDC15 results also demonstrate the utility of using a priori information for regime selection.

AMTD
8, 9959–9992, 2015

4.2 Case 2

Gaussian-distributed noise with a standard deviation of 0.5 K was added to the simulated brightness temperatures for this second case. The value was chosen to be consistent with the noise equivalent differential temperature for the MHS instruments (see Table 1). Perfect a priori information was provided to the retrievals.

Figure 4 compares the PLDC15 and MH08 mid regime retrievals to the input water vapour column. The standard deviations are increased compared to case 1, but more so for PLDC15 (see Table 3). Nevertheless, the standard deviation for MH08 is 78 % greater than for PLDC15.

In this case, the reduction of standard error by PLDC15 over MH08 is due primarily to the calculation of bias coefficients. In the extended regime, however, iterations account for 24 % of the overall correction.

Table 3 summarizes the results for the low, mid, and extended regimes. In each case the PLDC15 retrieval has a smaller standard deviation and bias. PLDC15's standard deviation is significantly lower for combined regimes, although this is partly due to the improved regime selection of PLDC15. The results indicate that the PLDC15 retrieval is more accurate.

4.3 Case 3

In the third case a climatological a priori is provided, which is the worst-case scenario for our retrieval. The climatological water vapour and temperature profiles were obtained by averaging the profiles from all 1490 measurements considered in this study. The noise and MH08 retrievals are the same as for Case 2.

Figure 5 compares the PLDC15 retrieval to the input water vapour column for the mid regime. The standard deviation is considerably increased, but is only marginally larger than for MH08 (see Table 3). The low regime is equal to the MH08 retrieval. For the extended regime, our retrieval performs slightly better in terms of standard deviation,

AMTD
8, 9959–9992, 2015

however, the bias is significantly larger than MH08. The results show that when the a priori is degraded our retrieval can be expected to perform comparably to MH08.

4.4 Assessment of PLDC15 assumptions

In this section we assess the following approximations employed in the development of the PLDC15 retrieval:

i. we ignored the second term of Eq. (3), which contains the difference between the surface air and skin temperatures, $T_o - T_s$; and

ii. we assume a specific value for the surface reflectance in Eq. (6) which may be in error.

To evaluate the impact of (i), we performed the same simulations from Case 1 using $T_o - T_s = \pm 5$ K. The same test was performed by MH08. Note that although atmospheric reanalyses often disagree on $T_o - T_s$, values up to 2 K are typical for Arctic sea ice (multi-year ice) (Melsheimer and Heygster, 2008). As such, this test represents an extreme case.

We found that inclusion of $T_o - T_s$ in the simulations caused a bias in the retrieved water vapour columns. The bias was positive for $T_o - T_s > 0$ and negative for $T_o - T_s < 0$. The bias varied for each regime in the retrieval. The low regime bias ranged from 3 to 5 % with increasing water vapour column. Similarly the mid regime bias ranged from 4 to 7 % and the extended regime bias ranged from 3 to 4 %. The scatter in the bias was less than 1 % in each case. For typical $T_o - T_s$ values of 2 K we can conclude that the errors introduced by the approximation (i) are less than 3 %.

For approximation (ii) we tested extreme values of the surface reflectivity. Applying the PLDC15 retrieval to simulations with surface refletances of 0.05 and 0.35 (Selbach, 2003), which represented the extremes in the Arctic, indicated that a value of 0.12 was optimal for the reflectance term in Eq. (6). A random error of less than 3 % in the water

AMTD
8, 9959–9992, 2015

column was induced by assuming a constant value of surface reflectance compared to the range of values seen from the SEPOR/POLEX campaign.

4.5 Evaluation of MH08 applied to MHS measurements

The MH08 retrieval was designed for application to AMSU-B measurements. Section 5, however, applies the MH08 retrieval to MHS brightness temperatures instead. The retrieval error can be assessed using the simulations from Case 1.

Table 4 shows the results when MH08 is applied to simulated MHS and AMSU-B brightness temperatures for each regime. In the low regime both the standard deviation and bias remain small. The mid regime's bias effectively changes sign and the standard deviation increases by 5 %. For the extended regime the standard deviation increases by 12 % whereas the absolute bias increased by 200 %. We conclude that the MH08 retrieval can be reasonably applied to MHS measurements for the low and mid regimes.

The simulations do not account for the difference in polarization measured by the two instruments. This has an unknown effect on the retrieved columns.

5 Measurements

This section examines PLDC15 water vapour columns retrieved from MHS overpasses of Barrow, Alaska, and compares them with simultaneous GVR measurements at Barrow. A variety of other data sets are also compared. Swath data are used to demonstrate the spatial distribution of the water vapour column.

5.1 Overpasses at Barrow, Alaska

A total of 11 546 measurements by MetOP-A and NOAA-18 within 50 km of Barrow, Alaska were obtained for the same time period as in Sect. 4. We retrieved water vapour columns from these data using PLDC15 with the ECMWF interim reanalysis as the a priori. The resolution of the ECMWF data is 80 km in latitude and reanalyses are

AMTD
8, 9959–9992, 2015

provided 4 times a day. Therefore, the PLDC15 retrievals have a priori information no more than 3 h from the overpass time of the MHS.

For the reflectance ratio in the mid regime we chose $r_1/r_2 = 1.12$ from SEPOR/POLEX data which is representative of ice and open water (Selbach, 2003). For the extended regime, we chose $r_1/r_2 = 1.19$ for a mixture of coastal ice and snow-covered land using MACSI aircraft campaign data (Hewison and English, 1999). The second ratio was chosen to be $r_2/r_3 = 1.12$ as these are the same frequencies as r_1/r_2 from the mid regime.

Figure 6 shows the results of the PLDC15 retrieval compared to coincident GVR measurements in terms of water vapour column. Since the GVR provides near-continuous measurements, they are averaged over three minutes to reduce instrument noise.

For the full data set the standard deviation is 0.72 kg m^{-2} and the bias is 0.01 kg m^{-2}. Note, however, that the error is larger at water vapour columns greater than 6 kg m^{-2}. The standard deviation and bias for GVR comparisons less than 6 kg m^{-2} are reduced to 0.39 and 0.08 kg m^{-2}, respectively. During the dry Arctic winter the water vapour column is rarely greater than 6 kg m^{-2} (Serreze and Barry, 2005).

Table 5 provides a statistical comparison of various water vapour data sets with the GVR, all for GVR-measured columns less than 6 kg m^{-2}. Reanalysis data sets include the European Centre for Medium-Range Weather Forecasts (ECMWF) Interim Product (Dee et al., 2011), the National Centers for Environmental Prediction (NCEP) (Kalnay et al., 1996) product, the Arctic System Reanalysis (ASR) (Bromwich et al., 2010), and the Japanese 55 year Reanalysis (JRA-55) (Kobayashi et al., 2015). Atmospheric Infrared Sounder (AIRS) (Divakarla et al., 2006) satellite data include three different products: infrared measurements, microwave measurements (using AMSU-A), and combined (infrared and microwave) measurements. The Microwave Integrated Retrieval System (MIRS) (Boukabara et al., 2010) is a data product that uses a one dimensional variational inversion scheme (1D-VAR) in conjunction with satellite measurements from MHS and AMSU sensors to determine atmospheric quantities such

AMTD
8, 9959–9992, 2015

as water vapour column. The MH08 retrieval is listed twice in Table 5 as it was used to determine the water vapour column from both the AMSU-B and MHS brightness temperatures.

From the results in Table 5, the standard deviation is smallest for the PLDC15 and JRA retrievals, although the JRA data set has a large negative bias. ECMWF and ASR standard deviations are only slightly larger. This is not surprising, given that the reanalyses incorporate data from radiosonde launches at Barrow. The MHS measurements, however, have considerably higher resolution, and so reveal more structure, as will be demonstrated in Sect. 5.2. It is also unclear how the measurements and analyses compare away from the radiosonde anchor points, and this is the subject of ongoing work.

The MH08 retrieval has a significantly larger standard deviation than PLDC15: 146 % greater when using AMSU-B, and 84 % greater for MHS. These results are broadly consistent with our conclusions using simulations in Sect. 4. Note that AMSU-B has intrinsically more noise than MHS (Table 1).

Table 6 provides a statistical comparison of using different data sets as the a priori for the PLDC15 retrieval compared with the GVR at Barrow. GVR water vapour columns of less than 6 $\mathrm{kg\,m^{-2}}$ are used again. The results from Table 6 show the standard deviation only slightly changing depending on the data set used for the a priori. The ECMWF PLDC15 retrieval has the smallest standard deviation compared to the other data sets while the NCEP data set gives the largest standard deviation. To use the ECMWF climatological profiles as the a priori, the daily ECMWF reanalysis was used for the regime selection.

5.2 Spatial plots of water vapour column

As an example of how PLDC15 can be applied to swath data, Fig. 7a shows the retrieval for the NOAA-18 MHS measurement from 1 February 2008. The area chosen is centered over the Chukchi Sea north of Alaska. The ECMWF interim reanalysis was used for the a priori, and the reflectance ratios from Sect. 5.1 were used for simplicity.

AMTD
8, 9959–9992, 2015

A detailed analysis of the Arctic-wide, emissivity-dependent PLDC15 retrieval is left for future work.

The plot shows individual footprints which vary in size due to the MHS's viewing angle. For comparison, Fig. 7b shows the equivalent ASR water vapour column for the same period. The ASR resolution is 30 km in latitude. The comparison reveals PLDC15 applied to MHS data has the higher intrinsic resolution. The ASR retrieval tends to smooth out fine details in the water vapour column.

5.3 Uncertainties

The PLDC15 errors in the measurements of Sect. 5 were greater than were obtained for the simulations in Sect. 4. This is not unexpected. Sources of error that exist in the overpass measurements that are not simulated include:

i. differences in the scene viewed by GVR and MHS;

ii. uncertainties in the reflection ratio terms in the mid and extended regimes;

iii. removal of the second term in Eq. (3);

iv. uncertainties in the a priori temperature profile;

v. changes with time in MHS noise equivalent differential temperatures;

vi. polarization in the MHS measurements for different frequencies;

vii. optically-thick ice crystal affecting MHS brightness temperatures;

viii. uncertainties in the GVR measurements; and

ix. the assumption of purely specular reflecting surface.

The error in (i) arises from the GVR being a stationary zenith-pointing instrument while the satellite-borne MHS has varying downward-pointing viewing angles. The criteria for an overpass match in Sect. 5 allows the centre of the MHS footprint to be

AMTD
8, 9959–9992, 2015

up to 50 km from Barrow, Alaska. Any geophysical variation in the water vapour field can be expected to result in differences between the two measurements. The viewing geometry error can potentially be larger than the random error from either instrument (Buehler et al., 2012).

The error in (ii) depends on the regime and frequencies selected. SEPOR/POLEX data show a high correlation for the 157 and 183 GHz surface emissivity measurements over different sea ice types. The high correlation corresponds to a small range of 0.96 to 1.12 for the reflectance ratio (r_1/r_2 for mid, r_2/r_3 for extended) over different types of sea ice and water surfaces. The 89 and 157 GHz surface emissivity measurements have very little correlation thereby producing a large range of 0.6 to 1.25 for the reflectance ratio (r_2/r_3 for extended). The range of r_1/r_2 for the mid regime term translates to a variation in the water vapour column of 25 %. Similarly, in the extended regime, the range of r_2/r_3 results in a variation of 35 %, and the large range of r_1/r_2 yields a variation of 175 %.

For (iii), the removal of the second term in the retrieval equation typically translates to a change of 3 % in water vapour column (as discussed in Sect. 4.4). Error from optically thick ice clouds in (vii) is expected to have little impact since wintertime Arctic ice paths are generally small (Miao et al., 2001). The error of the GVR measurements in (viii) is ±5 %. Other sources of error are difficult to quantify.

6 Conclusions

A new retrieval based on the microwave formulation developed by Miao was introduced. Simulations show that the new technique reduces errors compared to earlier approaches if a priori information for the atmospheric conditions is used. In a comparison with ground-truth measurements, the new PLDC15 retrieval provides more accurate water vapour columns than other satellite measurements having a standard deviation of 0.39 kg m^{-2} and a bias of 0.08 kg m^{-2}, and better resolution than atmospheric analysis data products.

AMTD
8, 9959–9992, 2015

Maps of water vapour can be created that reveal fine structure that conventional reanalyses are unable to discern. Pan-Arctic water vapour charts can be created twice per day using the combination of overpasses from NOAA-18 and MetOP-A alone. Temporal resolution may be further improved by including additional instruments. Given historical satellite data sets and planned launches, microwave water vapour measurements may provide new insights into the changes in Arctic climate.

The PLDC15 retrieval may be employed for a variety of purposes. It can be used to improve water vapour in reanalysis data sets, and to improve the initialization of water vapour in numerical weather prediction models. It may also be used for research purposes such as for the construction of Arctic water budgets.

Acknowledgements. The National Oceanic and Atmospheric Administration (NOAA) and the European Organisation for the Exploitation of Meteorological Satellites (EUMETSAT) provided Microwave Humidity Sounder (MHS) data from the NOAA and MetOP series satellites. Satellite Application Facility for Numerical Weather Prediction (NWP SAF) for providing the RTTOV radiative transfer model. The Atmospheric Radiation Measurement (ARM) program for supporting the G-band Vapor Radiometer (GVR). The Goddard Earth Sciences Data and Information Services Center (GES DISC) for providing the (Atmospheric Infrared Sounder (AIRS) data set. The European Centre for Medium-Range Weather Forecasts (ECMWF) for providing ERA-Interim data set. The Japan Meteorological Agency (JMA) for allowing access to the Japanese 55 year Reanalysis (JRA-55) data set. NOAA/OAR/ESRL PSD from Boulder Colorado, USA for providing the National Centers for Environmental Prediction (NCEP) reanalysis data. The Polar Meteorology Group from Ohio State University for providing the Arctic System Reanalysis (ASR) data set.

References

Boukabara, S., Garrett, K., and Chen, W.: Global Coverage of Total Precipitable Water Using a Microwave Variational Algorithm, IEEE T. Geosci. Remote, 48, 3608–3621, 2010. 9973

Bromwich, D., Kuo, Y., Serreze, M., Walsh, J., Bai, L., Barlage, M. Hines, K., and Slater, A.: Arctic system reanalysis: call for community involvement, EOS T. Am. Geophys. Un., 91, 13–14, 2010. 9973

AMTD

8, 9959–9992, 2015

Buehler, S. A., Östman, S., Melsheimer, C., Holl, G., Eliasson, S., John, V. O., Blumenstock, T., Hase, F., Elgered, G., Raffalski, U., Nasuno, T., Satoh, M., Milz, M., and Mendrok, J.: A multi-instrument comparison of integrated water vapour measurements at a high latitude site, Atmos. Chem. Phys., 12, 10925–10943, doi:10.5194/acp-12-10925-2012, 2012. 9976

Cadeddu, M., Turner, D., and Liljegren, J.: A neural network for real-time retrievals of PWV and LWP from Arctic millimeter wave ground based observations, IEEE T. Geosci. Remote, 9, 1887–1900, 2009. 9961

Dee, D., Uppala, S., Simmons, A., Berrisford, P., Poli, P., Kobayashi, S., Andrae, U., Balmaseda, M., Balsamo, G., Bauer, P., Bechtold, P., Belijaars, A., van de Berg, L., Bidlot, J., Bormann, N., Delsol, C., Dragani, R., Fuentes, M., Geer, A., Haimberger, L., Healy, S., Hersbach, H., Hólm, E., Isaksen, L., Kållberg, P., Köhler, M., Matricardi, M., McNally, A., Monge-Sanz, B., Morcrette, J., Park, B., Peubey, C., de Rosnay, P., Tavolato, C., Thépaut, J., and Vitart. F.: The ERA interim reanalysis: configuration and performance of the data assimilation system, Q. J. Roy. Meteor. Soc., 137, 553–597, 2011. 9973

Divakarla, M., Barnet, C., Goldberg, M., McMillin, L., Maddy, E., Wolf, W., Zhou, L., and Liu, X.: Validation of atmospheric infrared sounder temperature and water vapor retrievals with matched radiosonde measurements and forecasts, J. Geophys. Res., 111, D09S15, doi:10.1029/2005JD006116, 2006. 9973

Guissard, A. and Sobieski, P.: A simplified radiative transfer equation for application in ocean microwave remote sensing, Radio Sci., 29, 881–894, 1994. 9962

Hewison, T. and English, S.: Airborne retrievals of snow and ice surface emissivity at millimeter wavelengths, IEEE T. Geosci. Remote, 37, 1871–1879, 1999. 9973

Kalnay, E., Kanamitsu, M., Kistler, R., Collins, W., Deaven, D., Gandin, L., Iredell, M., Saha, S., White, G., Woollen, J., Zhu, Y., Leetmaa, A., Reynolds, R., Chelliah, M., Ebisuzaki, W., Higgins, W., Janowiak, J., Mo, K. C., Ropelewski, C., Wang, J., Jenne, R., and Joseph, D.: The NCEP NCAR 40 year reanlysis project, B. Am. Meteorol. Soc., 77, 437–470, 1996. 9973

Kleepsies, T. and Watts, P.: Comparison of simulated radiances, Jacobians and linear error analysis for the microwave humidity sounder and the advanced microwave sounding unit B, Q. J. Roy. Meteor. Soc., 132, 3001–3010, 2006. 9980

Kobayashi, S., Ota, Y., Harada, Y., Moriya, M., Onoda, H., Onogi, K., Kamahori, H., Kobayashi, C., Endo, H., Miyaoka, K., and Takahashi, K.: The JRA 55 reanalysis: general specifications and basic characteristics, IEEE T. Geosci. Remote, 93, 5–48, 2015. 9973

AMTD
8, 9959–9992, 2015

Lesins, G., Duck, T., and Drummond, J.: Climate trends at Eureka in the Canadian high Arctic, Atmos. Ocean, 48, 59–80, 2010. 9967

Lesins, G., Duck, T., and Drummond, J.: Surface energy balance framework for Arctic amplification of climate change, J. Climate, 25, 8277–8288, 2012. 9967

Matricardi, M. and Saunders, R.: Fast radiative transfer model for simulation of infrared atmospheric sounding interferometer radiances, Appl. Optics, 38, 5679–5691, 1999. 9966

Melsheimer, C. and Heygster, G.: Improved retrieval of total water vapor over polar regions from AMSU-B microwave radiometer data, IEEE T. Geosci. Remote, 46, 2307–2322, 2008. 9961, 9963, 9971

Miao, J.: Retrieval of Atmospheric Water Vapor Content in Polar Regions Using Spaceborne Microwave Radiometry, Alfred Wegener Inst. Polar Marine Res., Bremerhaven, Germany, 1998. 9961, 9963

Miao, J., Kunzi, K., Heygster, G., Lachlan-Cope, T., and Turner, J.: Atmospheric water vapor over Antarctica derived from special sensor microwave/temperature 2 data, J. Geophys. Res., 106, 10187–10203, 2001. 9960, 9964, 9976

Selbach, N.: Determination of Total Water Vapor and Surface Emissivity of Sea Ice at 89 GHz, 157 GHz and 183 GHz in the Arctic Winter, PhD thesis, University of Bremen, Bremen, Germany, 2003. 9971, 9973

Serreze, M. and Barry, R.: The Arctic Climate System, Cambridge University Press, Cambridge, UK, 2005. 9973

Serreze, M., Barry, R., and Walsh, J.: Atmospheric water vapor characteristics at 70 N, J. Climate, 8, 719–731, 1995. 9960

Stamnes, K., Ellingson, R., Curry, J., Walsh, J., and Zak, B.: Review of science issues, deployment strategy, and status for the ARM north slope of Alaska-Adjacent Arctic Ocean Climate Research Site, J. Climate, 12, 46–63, 1998. 9960

AMTD
8, 9959–9992, 2015

Table 1. AMSU-B and MHS instrument specifications including frequencies, noise equivalent differential temperature, and nadir polarization orientations (Kleepsies and Watts, 2006). Entries like 183.31 ± 3 GHz imply that two frequency bands at 182.31 and 184.31 GHz are combined. Vertical and horizontal polarization refers to cross-track and along-track polarization respectively.

Frequencies (GHz)		Noise (K)		Polarizations	
AMSU-B	MHS	AMSU-B	MHS	AMSU-B	MHS
89	89	0.40	0.32	Vertical	Vertical
150	157	0.80	0.53	Vertical	Vertical
183.31 ± 1	183.311 ± 1	0.80	0.50	Vertical	Horizontal
183.31 ± 3	183.311 ± 3	0.75	0.41	Vertical	Horizontal
183.31 ± 7	190.311	0.80	0.55	Vertical	Vertical

AMTD
8, 9959–9992, 2015

Table 2. MHS frequencies for the low, mid, and extended regimes for the retrievals of water vapour column with typical water vapour column ranges. The frequencies ν_1,ν_2,ν_3 in each regime are ordered so that $\tau_1 < \tau_2 < \tau_3$.

Regime	Frequencies (GHz) (MHS)			W Range (kg m^{-2})
	ν_1	ν_2	ν_3	
Low	190.311	183.311 ± 3	183.311 ± 1	0–2.5
Mid	157	190.311	183.311 ± 3	1.5–9
Extended	89	157	190.311	8–15

AMTD
8, 9959–9992, 2015

Table 3. Standard deviation (SD) and bias ($kg\,m^{-2}$) for PLDC15 and MH08 retrievals from simulated signals for the low, mid and extended regimes (excluding overlap). Results from three cases are provided. Case 1 uses noiseless simulated brightness temperatures with a perfect a priori. Case 2 uses simulated brightness temperatures with gaussian noise and a perfect a priori. Case 3 uses simulated brightness temperatures with gaussian noise and a climatological a priori. Case 3 does not include a column for combined measurements because regime selection requires better a priori information.

	Low		Mid		Extended		Combined	
Case 1	SD	Bias	SD	Bias	SD	Bias	SD	Bias
PLDC15	0.00	0.00	0.00	0.01	0.00	0.07	0.01	0.01
MH08	0.08	0.10	0.35	−0.10	0.57	−0.67	0.67	0.13
Case 2								
PLDC15	0.10	0.00	0.23	0.03	0.34	−0.11	0.19	0.02
MH08	0.13	0.10	0.41	−0.07	0.68	−0.63	0.64	0.12
Case 3								
PLDC15	0.13	0.05	0.44	−0.13	0.59	−1.23	n/a	n/a
MH08	0.13	0.10	0.41	−0.07	0.68	−0.63	n/a	n/a

AMTD
8, 9959–9992, 2015

Table 4. Standard deviation (SD) and bias ($kg\,m^{-2}$) for MH08 retrievals from simulated signals for the low, mid and extended regimes (excluding overlap). The AMSU-B results are the same as in Case 1 from Table 3.

Retrieval	Low		Mid		Extended	
	SD	Bias	SD	Bias	SD	Bias
AMSU-B	0.07	0.08	0.35	−0.11	0.57	−0.66
MHS	0.07	0.04	0.37	0.09	0.64	1.97

AMTD
8, 9959–9992, 2015

Table 5. Water vapour column comparisons of other data sets and retrievals to GVR retrievals at values less than 6 kg m^{-2} at Barrow, Alaska.

Data set/Retrieval		Nadir Resolution (km)	Standard deviation (< 6 kg m^{-2})	Bias (< 6 kg m^{-2})
AIRS	Combined	45	1.03	−0.34
	Infrared		1.10	−0.22
	Microwave		1.05	0.11
NCEP		280	0.79	−0.04
JRA		140	0.39	−0.49
ECMWF		80	0.42	−0.11
ASR (≤ 2012)		30	0.40	−0.18
MIRS (MHS 2014)		15	0.69	−0.18
MH08 (AMSU-B ≤ 2009)		15	0.95	0.20
MH08 (MHS)		15	0.71	0.23
PLDC15 (MHS)		15	0.39	0.08

AMTD
8, 9959–9992, 2015

Table 6. Water vapour column comparisons using the PLDC15 retrieval with different a priori data sets.

A Priori	Standard deviation ($< 6\,kg\,m^{-2}$)	Bias ($< 6\,kg\,m^{-2}$)
AIRS Combined	0.41	−0.02
NCEP	0.51	0.20
JRA	0.44	0.16
ASR ($\leq$ 2012)	0.46	0.08
ECMWF	0.39	0.08
ECMWF (Climatological)	0.45	0.08

AMTD
8, 9959–9992, 2015

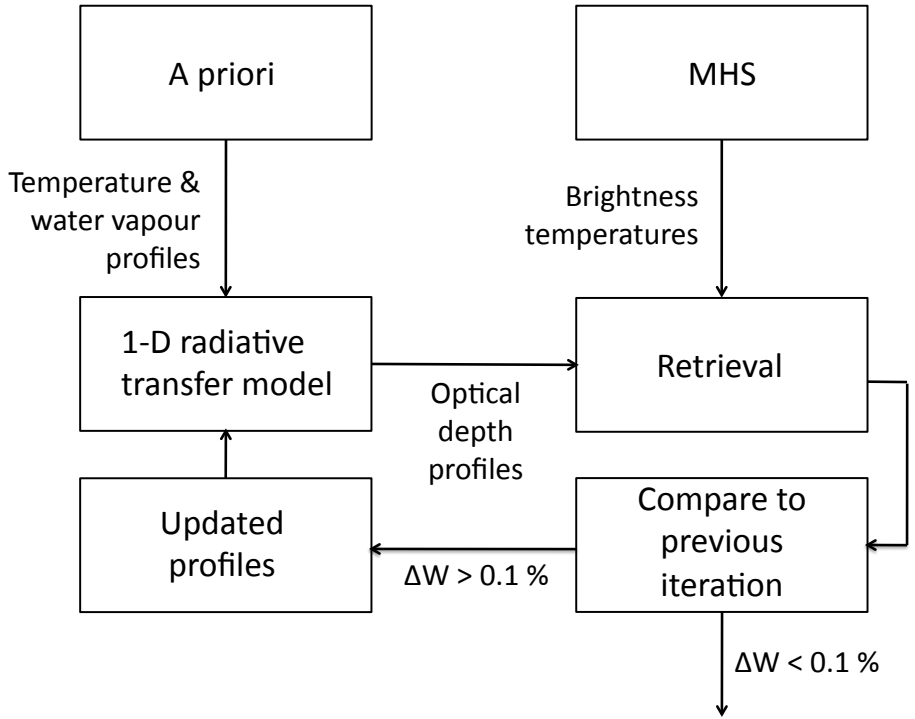

Figure 1. PLDC15 retrieval flow chart. The retrieval starts with a priori temperature, pressure and water vapour profiles input into the RTTOV 1-D radiative transfer model to produce optical depth profiles. These optical depth profiles and satellite brightness temperatures are used with Eqs. (2), (6) and (7) to produce a retrieval of the scaling factor x which is used to adjust the original water vapour profile through Eq. (9). This is repeated until convergence is achieved. The final water vapour column is given by Eq. (10).

AMTD
8, 9959–9992, 2015

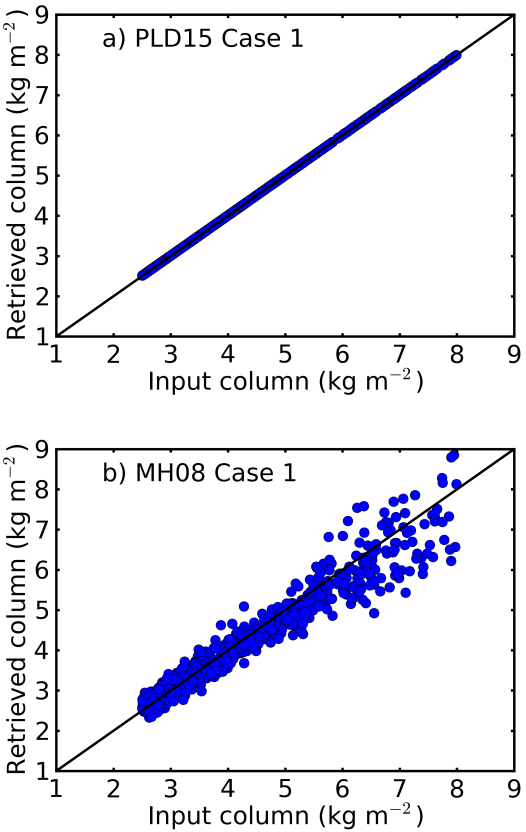

Figure 2. Comparisons of mid regime retrievals (excluding overlap) from simulated signals against the input water vapour columns for **(a)** PLDC15 and **(b)** MH08. The simulated signals are noiseless and perfect a priori information is provided. The black line represents a perfect retrieval.

AMTD
8, 9959–9992, 2015

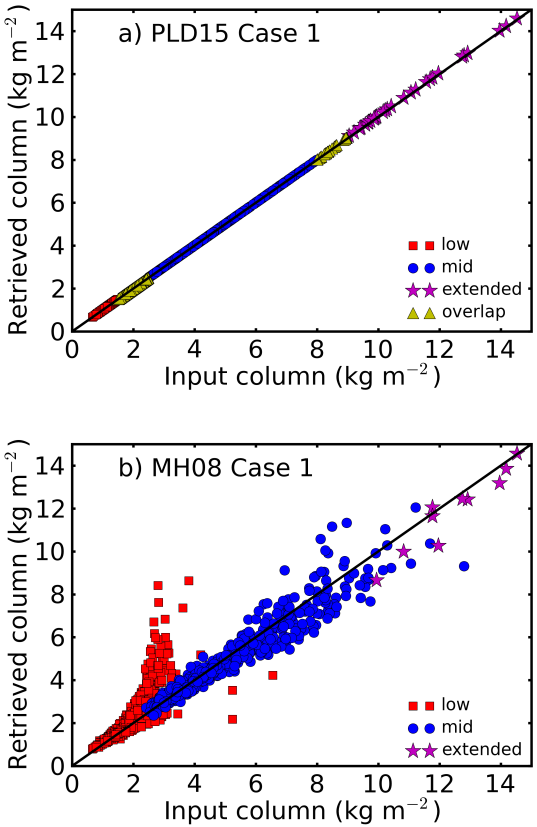

Figure 3. Comparisons of combined regime retrievals from simulated signals against the input water vapour columns for **(a)** PLDC15 and **(b)** MH08. The simulated signals are noiseless and perfect a priori information is provided. The black line represents a perfect retrieval.

AMTD
8, 9959–9992, 2015

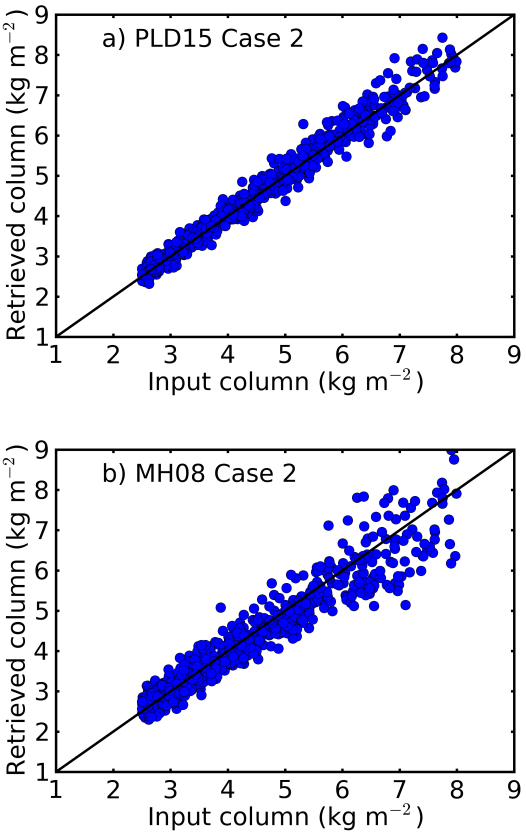

Figure 4. Comparisons of mid regime retrievals (excluding overlap) from simulated signals against the input water vapour columns for **(a)** PLDC15 and **(b)** MH08. The simulated brightness temperatures include gaussian noise with a 0.5 K standard deviation, and perfect a priori information is provided. The black line represents a perfect retrieval.

AMTD
8, 9959–9992, 2015

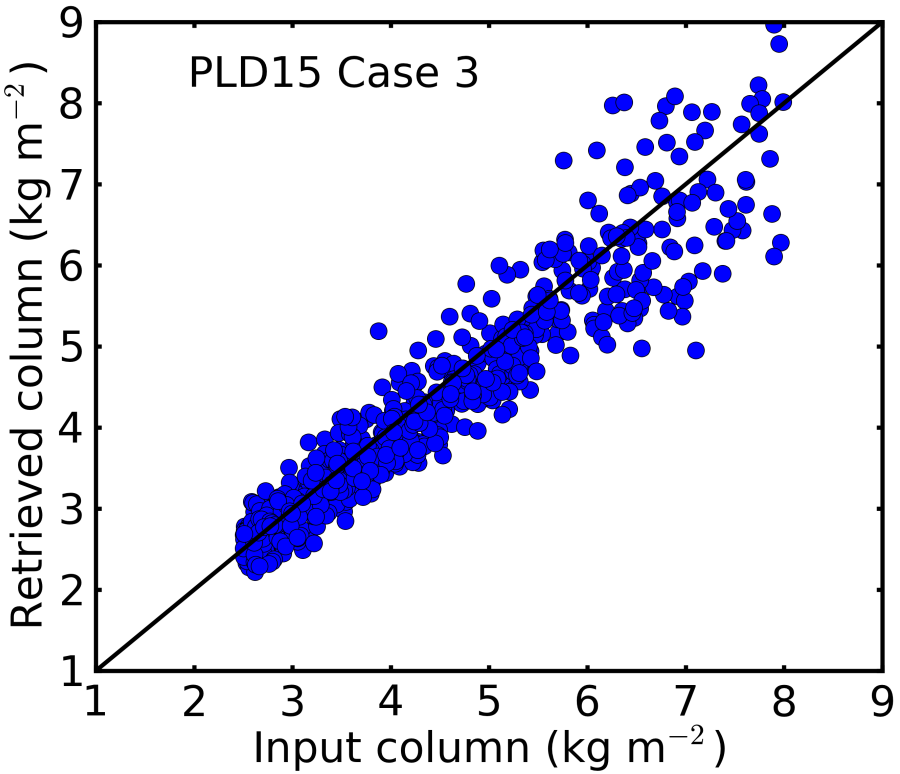

Figure 5. Comparison of the mid regime retrieval (excluding overlap) from simulated signals against the input water vapour columns for PLDC15. The simulated brightness temperatures include gaussian noise with a 0.5 K standard deviation, and climatological a priori information is used. The black line represents a perfect retrieval.

AMTD
8, 9959–9992, 2015

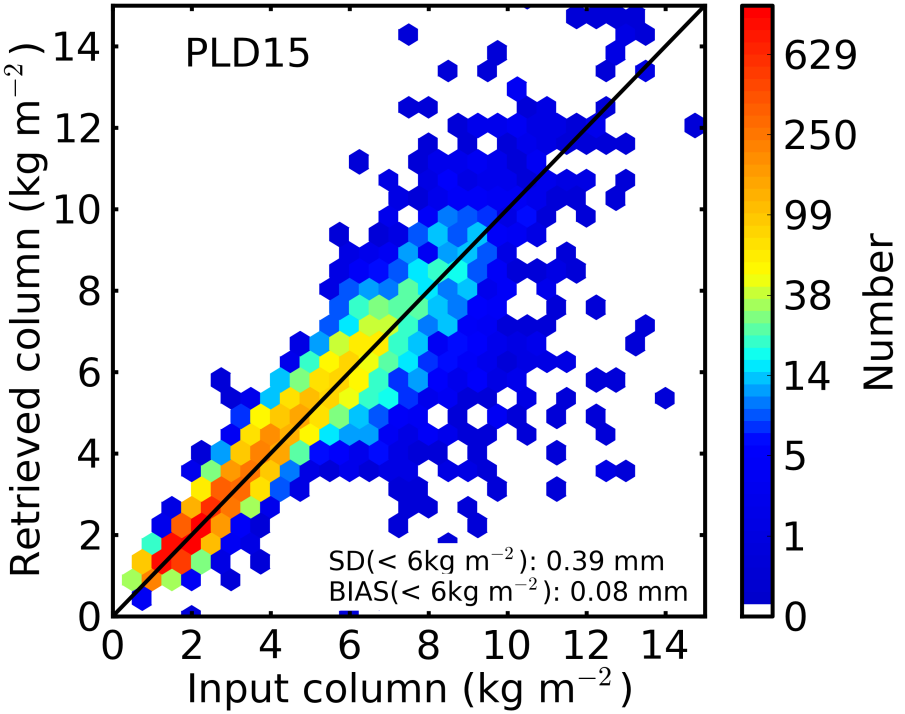

Figure 6. PLDC15 retrieval of water vapour column from MHS brightness temperatures compared to GVR retrievals at Barrow, Alaska.

AMTD
8, 9959–9992, 2015

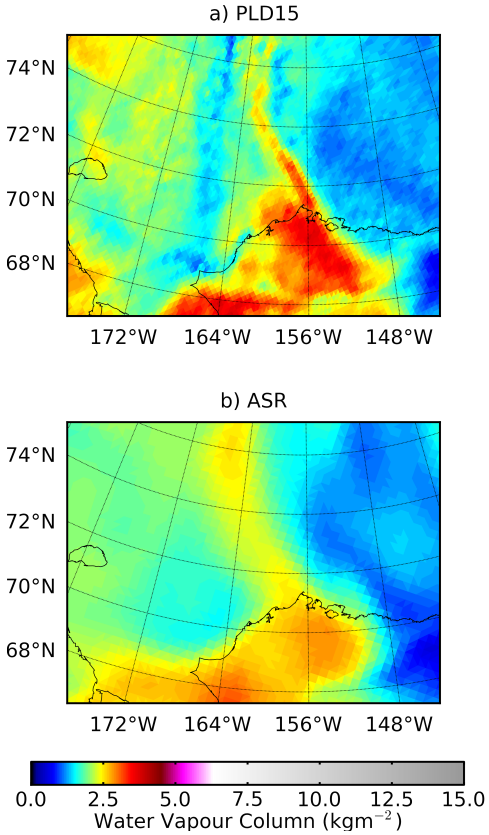

Figure 7. Spatial construction of water vapour column using the **(a)** PLDC15 retrieval using NOAA-18 MHS brightness temperature measurements over a region centred over the Chukchi Sea north of Alaska on 31 January, 23:09, 2008. and **(b)** the Arctic System Reanalysis (ASR) water vapour column data for 1 February 2008 at 00:00 UTC centred over Barrow, Alaska.

AMTD
8, 9959–9992, 2015